LASER INTERFEROMETER GRAVITATIONAL WAVE OBSERVATORY
- LIGO -
CALIFORNIA INSTITUTE OF TECHNOLOGY
MASSACHUSETTS INSTITUTE OF TECHNOLOGY

Document Type	**LIGO-T980086-00 - D**	9/22/98

Increased Thermal Noise in Nonuniform Fused Silica Suspension Fibers

Phil Willems and Mukund Thattai

Distribution of this draft:

Detector

This is an internal working note
of the LIGO Project..

California Institute of Technology
LIGO Project - MS 51-33
Pasadena CA 91125
Phone (626) 395-2129
Fax (626) 304-9834
E-mail: info@ligo.caltech.edu

Massachusetts Institute of Technology
LIGO Project - MS 20B-145
Cambridge, MA 01239
Phone (617) 253-4824
Fax (617) 253-7014
E-mail: info@ligo.mit.edu

WWW: http://www.ligo.caltech.edu/

1 ABSTRACT

Advanced versions of the LIGO detector are likely to use fused silica suspension fibers instead of the metal wires used in initial LIGO in order to take advantage of the lower internal loss of fused silica compared to metals. Unlike metallic wire, fused silica fibers used in suspensions typically have tapered regions at the ends of the flexible region, which is where the losses are concentrated in suspension motion. Since the losses of a fiber increase with its diameter, tapered fibers must have higher losses and higher thermal noise than uniform fibers. We calculated the thermal noise spectrum for fused silica fibers with dimensions and taper geometries typical of those used in gravitational wave detectors using a finite element analysis of a wire pendulum. The simulations show that within the range of fiber parameters we considered representative of suspensions currently in use, the increase in loss for a typical violin mode can be as much as a factor of 2, leading to roughly 1.4 times higher thermal noise in the interesting frequency range of 10-1000 Hz. The loss increase can be even larger for extreme nonuniformities. However, the effect can be easily managed by judicious fiber fabrication and attachment techniques and does not represent a critical barrier to the achievement of low thermal noise suspensions.

2 KEYWORDS

fused silica, suspensions, nonuniform, taper, mechanical loss, thermal noise

3 INTRODUCTION

The same intrinsically low internal mechanical loss that makes fused silica a good material for test mass mirrors also makes fused silica attractive as a suspension wire material. Compared to metals at room temperature, fused silica has internal losses roughly one hundred times lower in the frequency band of maximum sensitivity for LIGO. For this reason, fused silica is the currently preferred suspension wire material for advanced LIGO detectors.

Most of the research demonstrating the high performance of fused silica as well as its feasibility in actual suspensions has been done at the University of Glasgow by Jim Hough's group and at Moscow State University by Vladimir Braginsky's group (see, for example, [1-5]). These groups have used off-the-shelf optical fiber and pure fused silica fibers pulled either by hand or in a draw tower in their suspensions tests. Fibers made in the lab are clearly preferable, and the very best fibers have been drawn by hand using a hydrogen torch.

Unlike metal wires, fused silica fibers cannot be firmly clamped into suspension supports. Instead, the large-diameter endpieces left behind from the original rod are often left on the drawn fiber and are clamped, welded, or bonded to the suspension support and test mass. The small diameter fiber is thus connected to the large diameter endpieces by taper regions of some length and geometry determined by the fabrication process.

The thermal noise spectrum of a uniform wire pendulum is well understood. The case for a single wire pendulum has been analytically solved by Gonzalez and Saulson [6], and is consistent with a simpler conceptual model that predicts that the losses are concentrated in the portions of the wire with the most bending, namely the endpoints.

The losses of a wire pendulum can be simply related to the internal losses of the wire material by use of the *dilution factor*, which is the ratio of the lossless gravitational energy of the pendulum to its elastic energy. Since all the pendulum losses are due to elastic forces (assuming all other damping mechanisms are essentially eliminated by careful design), the losses for the pendulum are simply the loss of the material divided by the dilution factor.

The elastic energy of the pendulum is in turn a function of the wire diameter. The smaller the wire diameter, the less stiff it is and therefore the less elastic energy it stores during the pendulum oscillation. The gravitational energy is not dependent on the wire diameter except through the wire's mass, which is very small compared to the mirror mass and therefore ignorable. The gravitational energy instead depends on the wire length L. Therefore, the formula for a low loss pendulum is to maximize its length and minimize the diameter of the wire at its endpoints (leaving it thick enough to safely support the test mass, of course).

It is here that the manufacturing process of fused silica fibers interferes with their function, because it is precisely at the fiber endpoints that the diameter is increasing. This paper presents calculations that determine the reduction in Q due to these taper regions at the fiber endpoints.

4 THE PHYSICAL MODEL AND NUMERICAL ANALYSIS

The physical system modelled for this analysis is a single wire pendulum like that modelled by Gonzalez and Saulson [6]. A single wire of length L is rigidly clamped at its top end and supports a mass M with moment of inertia J at its bottom end. The wire has linear mass density ρ and moment of inertia I that are functions of position along the wire. Only motion in the x-direction- perpendicular to the test mass face- is considered. A detailed derivation of the equations of motion for the pendulum is given in Appendix 1.

The equations are analytically solvable for the uniform wire case, but for the general non-uniform wire case a numerical solution must be sought. Our approach was to model the wire as a discrete mesh of a few thousand points, thus reducing the complex fourth-order differential equation to eight coupled first-order difference equations for each point on the mesh, and then to iteratively improve a rough initial guess to the solution into conformance with the difference equations and boundary conditions using a relaxation technique, as described in Numerical Recipes in C [7]. Our first attempt at solution used a shooting technique to integrate the O.D.E. forward from a first guess at the top boundary of the fiber and see if the solution matched the bottom boundary; if not, the conditions at the first boundary were revised and the process repeated in a root-finding algorithm to find the lower boundary condition. This approach was overly sensitive to exponentially growing solutions and so was dropped.

The program performing these calculations was tested by calculating the solution of the uniform wire pendulum and comparing the result to the analytical solution. The two calculations yielded exactly the same answers for the mode shapes, strengths, and Q values for the various modes of the system to within the error expected for estimates of Q based on measurements at a finite set of frequencies. They also agreed on the size and slope of the background thermal noise spectrum. The precision of the calculations increased with decreasing mesh size, as expected (see Figure 1).

Figure 1: Integrated fractional error vs. number of mesh points, obtained by comparison of numerical and analytical solutions for a uniform wire pendulum.

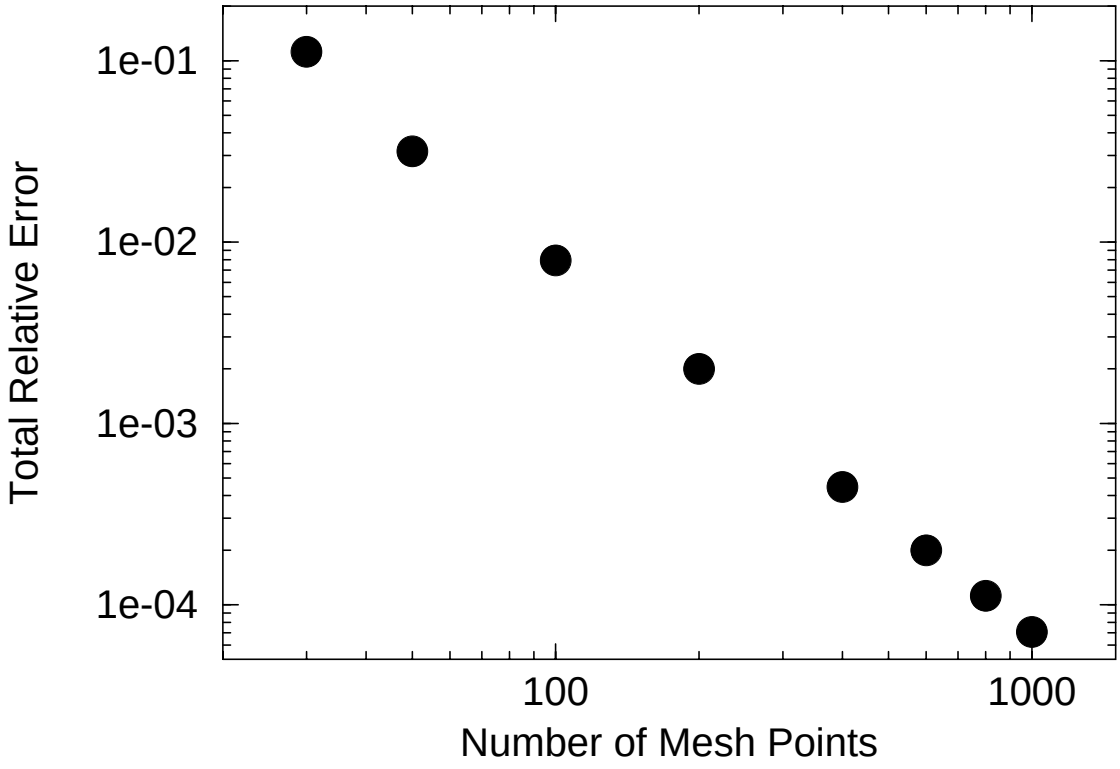

We also checked that the quality factor of the modes was inversely proportional to the loss in the wire material, as expected for $\phi<<1$. It was, over the three orders of magnitude for which we ran simulations, and so all the calculations shown here use $\phi=10^{-3}$, and can be extrapolated down to the 10^{-6} values typical for fused silica (see Figure 2). Calculations at lower values of Q are computationally more convenient because the relaxation algorithm uses the solution to the equations at one frequency as the initial guess for the solution at a nearby frequency; the higher the Q the more solutions at nearby frequencies will differ, making the initial guess poorer.

Figure 2: Dilution factor vs. loss factor ϕ for the third violin mode.

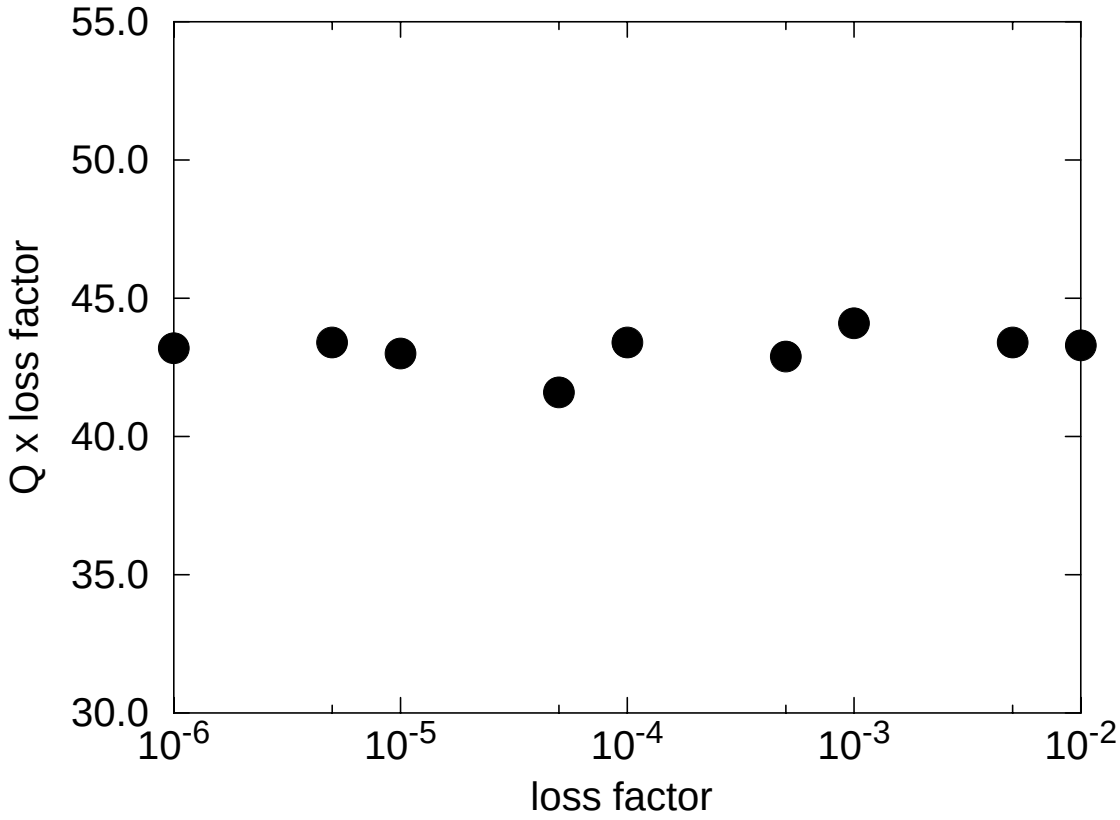

We considered three types of tapers in particular: linear, exponential, and inverse-square-root. All three are experimentally realizable using straightforward fiber pulling techniques, and they should apply in varying degrees to the fibers now being pulled in laboratories. The exponential taper is expected for a fiber pulled in a uniform hot zone of constant width. The inverse-square-root taper is expected for a fiber pulled in a draw tower with a uniform hot zone. The linear taper can be achieved by pulling a fiber in a hot zone that is uniform but whose size decreases at half the rate that the fiber is pulled. This last geometry is somewhat more more difficult to achieve but has been shown in the laboratory. As a numerical ideal it is a useful case to consider since the other geometries are linear to first order near the beginning of the taper. A more detailed derivation of these taper geometries can be found in Appendix 2. We wish to point out that even where experimental taper profiles differ from those studied here, the trends shown in this paper are expected to apply.

5 RESULTS OF THE SIMULATION

The fiber pendulum that we modelled for the nonuniform case was chosen to have parameters closely matching that used by Rowan et al. in their measurements of pendulum and violin mode Q's [1], the major difference being that our mass was chosen to be half as heavy than theirs since they used a two wire pendulum as opposed to our one wire pendulum and we wished to keep the diameters and wire strains similar.

We find that, for the set of taper geometries considered, the reduction in Q can be up to a factor of 2, or even more for tapers of extreme length. One comparison was to take the overall length of the fiber as fixed, as well as the diameters of the ends and inner region, and investigate the change in the Q and ω of the first violin mode as the length of the taper was varied. These data are shown in Figures 3 and 4. The overall fiber length is fixed at 30 cm, the radius of the flexible inner region of the fiber is fixed at 145 μm and the radius of the outer regions is 1.5 mm. The data for the exponential taper are very close to those for the linear taper and are not shown.

Figure 3: Dilution factors for tapered fibers as a function of taper length, with inner and outer radii fixed. The filled circles give the data for uniform fibers with length equal to the length between the taper regions. The open triangles and squares are the data for linear and inverse-square-root tapers, respectively.

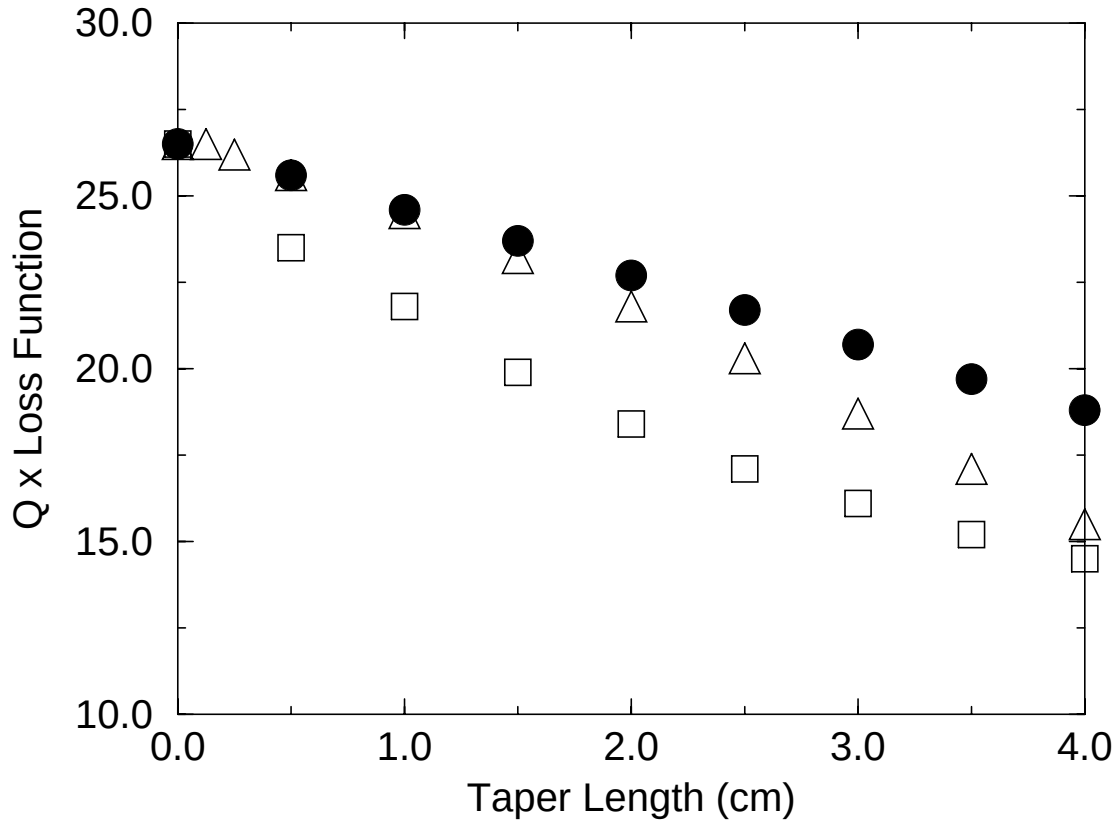

The Q of even a uniform fiber pendulum is expected to vary with length, since the gravitational energy of a mode is proportional to length while the elastic energy is concentrated at the end-points and largely insensitive to length. Therefore, a refinement to the naive assumption that the effective fiber length is that of the uniform region plus the tapers is to assume that the effective length is that of the uniform region alone. This is the model to which the simulation is compared in Figures 3 and 4. We can see that this picture helps us to understand the behavior of nonuniform pendulums, and that they fall short of ideal even in this picture.

Figure 4: Frequency of the first violin mode as a function of taper length, with inner and outer radii fixed. The symbols are the same as in Figure 3.

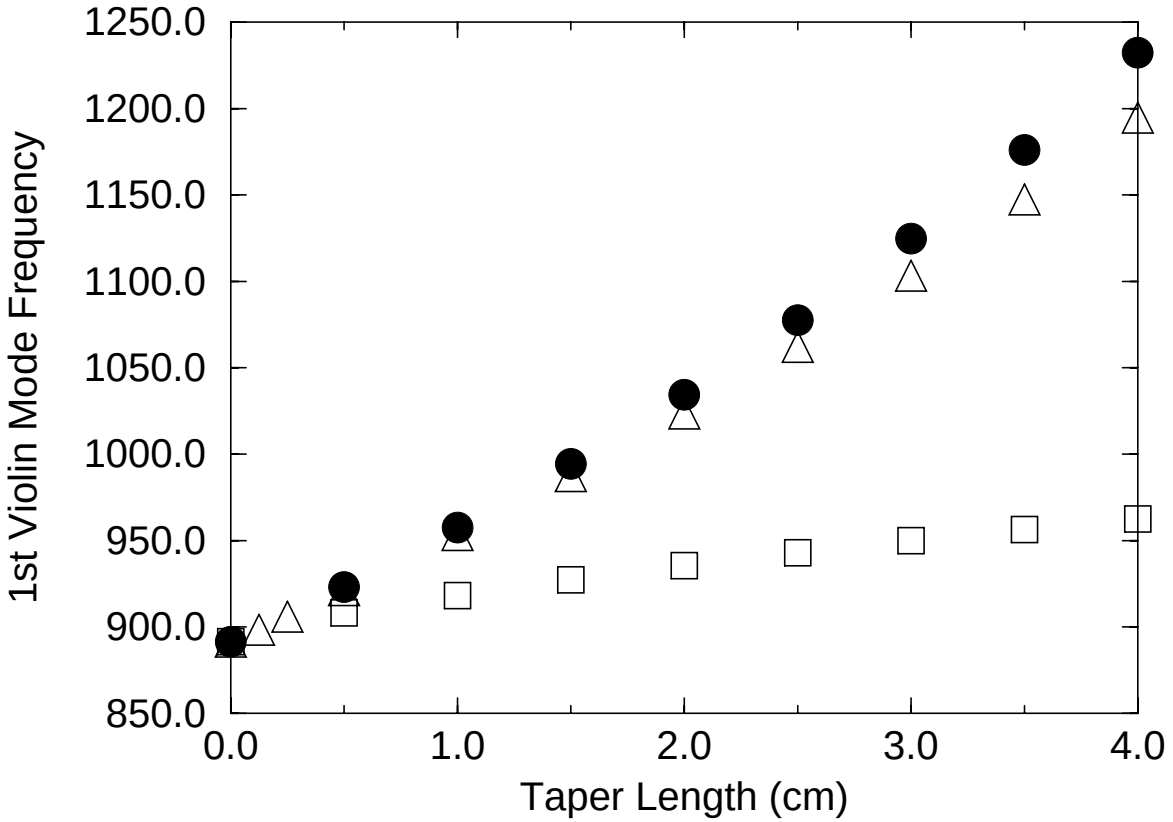

As the taper region is made longer, the uniform portion of the fiber is shorter, and the resonant frequency increases. However, the increase is less than expected based on just the length of the uniform region, so part of the taper region must be bending as well, and if the taper is bending, then the Q of the mode must be reduced. This is just what is seen. Notice that the inverse-square-root taper shows the greatest reduction in Q, along with the smallest change in ω. This is because the inverse-square-root taper tends to concentrate most of its change in radius near the end as its length increases, leaving a long gradual taper near the uniform section, This long gradual taper is relatively flexible despite its increased diameter and so causes a relatively large loss.

Another comparison is to leave the length of the taper region constant, and investigate the change in Q and ω due to a change in the outer diameter of the taper. This is equivalent to pulling the fiber from stock of different initial diameters. These data are shown in Figures 5 and 6. The data are given as function of the taper depth, defined as the difference between the inner and outer radii of the fiber (thus, zero taper depth would be no taper). The fiber length is again 30 cm and the inner radius 145 μm, and the taper length is fixed at 2 cm.

Figure 5: Dilution factors as a function of taper depth. The triangles and squares represent linear and inverse-square-root taper data as in Figure 4, and the diamonds represent exponential taper data. The dashed line is the limiting case of a uniform fiber with the tapers removed. The taper length is fixed at 2 cm.

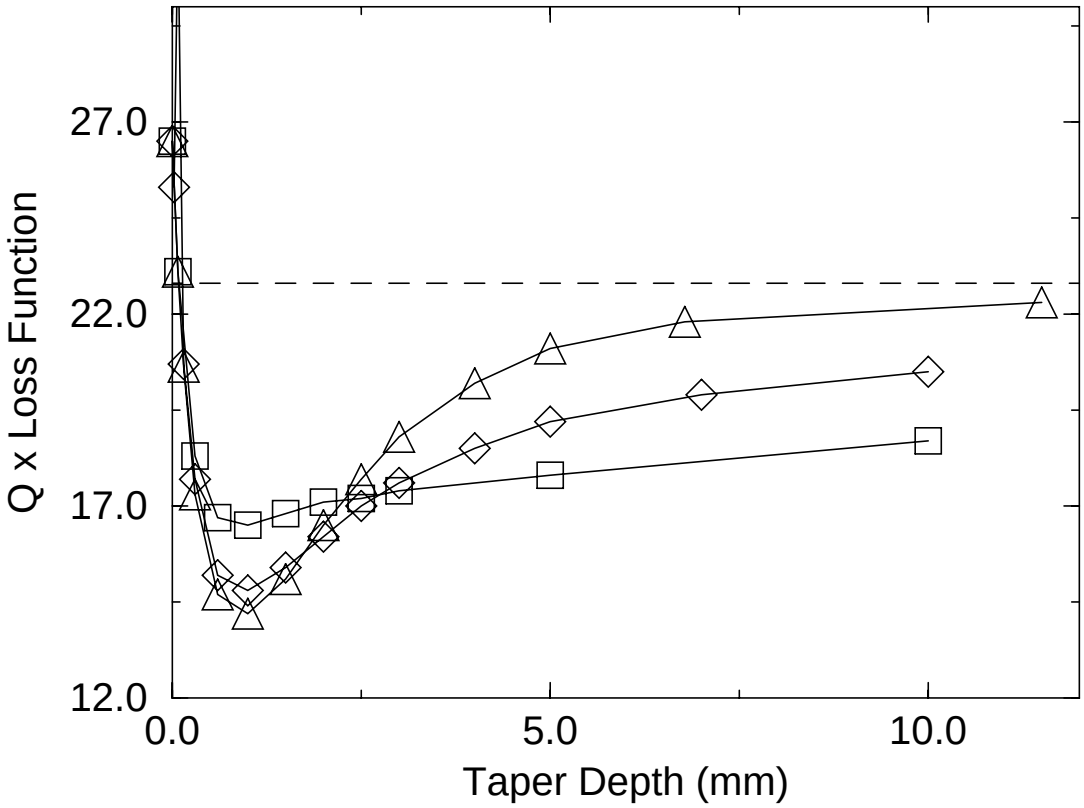

In this case, all three taper types start as uniform. As the taper depth (and thus angle) is increased, the linear and exponential tapers become increasingly abrupt, and the behavior of the fiber approaches that of a uniform fiber of the shorter length between the tapers. However, there is a taper angle where the Q becomes a minimum at about one-half the maximum Q. This is true for all taper styles, which resemble each other closely when the initial and final diameters are similar. This is where the increase in diameter is not large enough to exclude bending, but is large enough to induce excess loss. As the outside diameter increases further, more of the taper becomes too stiff to bend and the losses decrease.

The data at very large taper depths must be considered with some skepticism, for the equations of motion are based upon an assuption that the cone angle made by the tangent to the fiber surface is small, which is not obviously the case for taper depths as large as 10 mm in this model, where the cone angle is arctan(1/2)=.46 radians. However, the trends in the data are intuitively plausible. For the linear and exponential tapers, as the outer radius is increased the slope of the taper where it meets the slender inner part of the fiber also increases, and so the transition becomes increasingly abrupt. In the limit of a perfectly abrupt transition to an infinite plane- as the taper depth becomes very large- the system becomes that of a shorter uniform fiber clamped at its endpoints, and this is what the data show.

For the inverse-square-root taper, the slope of the taper where it meets the uniform part of the fiber saturates at a relatively small taper depth (see Appendix 2). As the taper depth is further increased, most of the change in fiber radius becomes concentrated near the outer portion of the taper, and so the length of the relatively uniform part of the fiber approaches a constant that is close to the overall length of the fiber. Thus, the resonant frequency of the fiber tends to stay close to the uniform fiber value. However, most of the taper is then close to being a gradual linear taper, which has relatively high loss, and so the loss of the inverse-square-root taper stays large. It is worth noting that the concentration of diameter increase makes the inverse-square-root taper more susceptible to breakdown of the small-angle approximation than the other two tapers.

Figure 6: Frequency of the first violin mode as a function of taper depth. The symbols are defined as in Figure 5. The dashed line represents the frequency of a uniform fiber of the length between the tapers

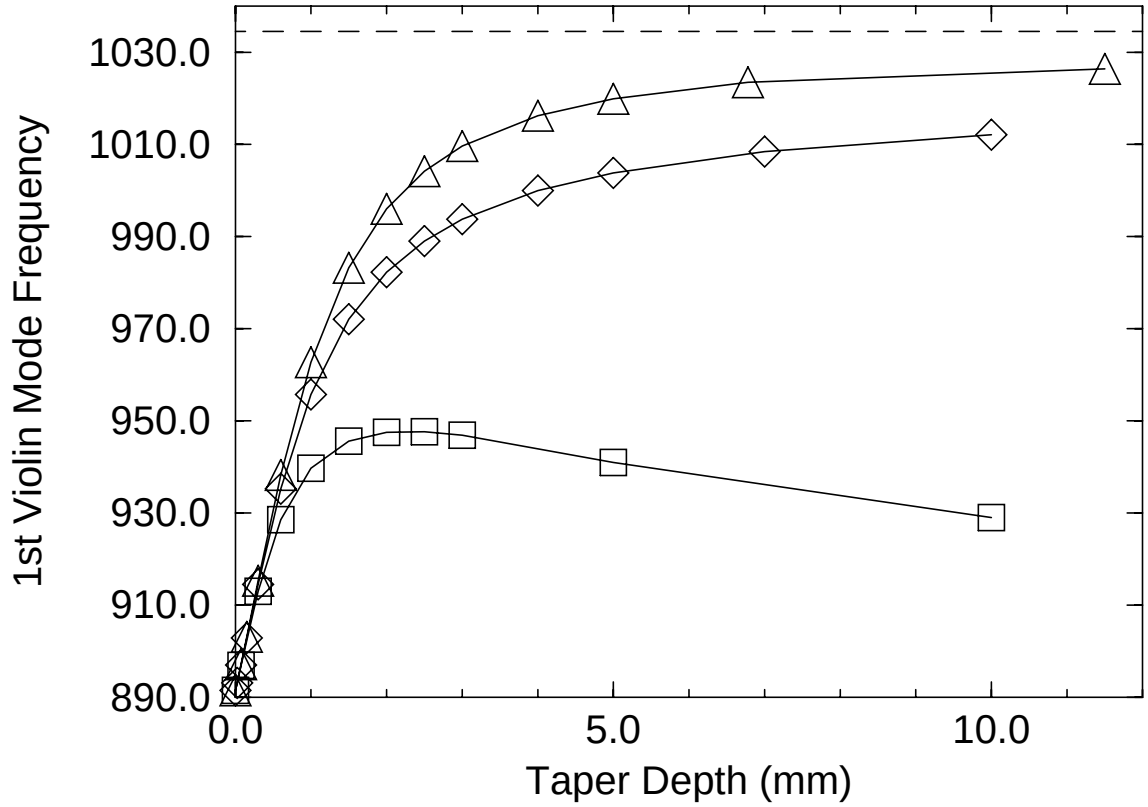

6 CONCLUSIONS

As expected, the reduction in Q for the resonant modes in the system is accompanied by an increase in the off-resonant thermal noise (see Figure 7). For the worst case shown above (although not the worst possible case), the thermal noise in the 5-100 Hz region is increased by a factor of 1.4 from the ideal uniform fiber case. This must therefore be considered a potentially important noise source.

The solutions suggested by this analysis are relatively simple to implement, however. The best Q's are obtained by giving the taper the largest possible linear slope at the point near the uniform region. Therefore, tapers should be short, end in a large diameter relative to the uniform region, and have linear- or exponential-like profiles. Fabricating fibers with small hot zones (in the case of the draw tower model) is one way to achieve this. Another is to utilize tailored torch oscillation routines as described by Birks and Li [8] to achieve arbitrary taper profiles. A third is to dispense with the tapers altogether and either weld or clamp the uniform parts of the fiber directly into the suspension.

Figure 7: Thermal noise spectrum for three suspensions. The dashed line is for a fiber with 2 cm linear tapers and a 26 cm uniform central region. The solid line is for a 26 cm uniform fiber without tapers. The dotted line is for a 30 cm uniform fiber without tapers. The tapers on the ends of the 30 cm fiber have increased the thermal noise by a factor of about 1.4.

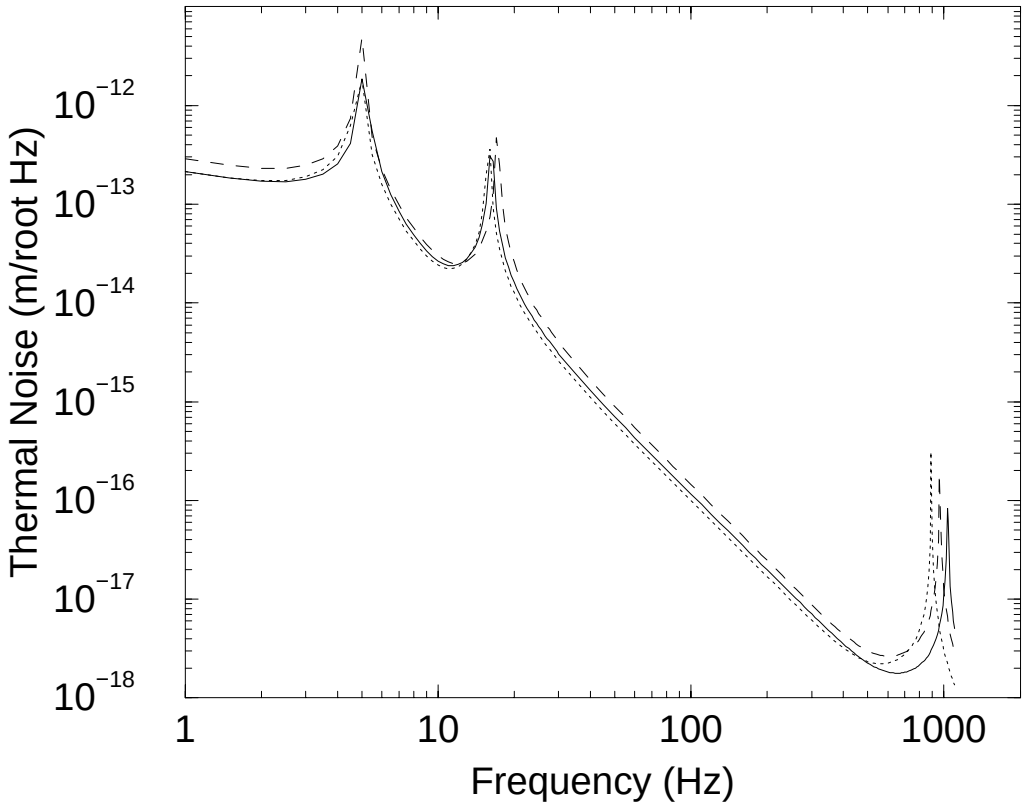

7 REFERENCES

1. "Q factor measurements on prototype fused quartz pendulum suspensions for use in gravitational wave detectors," S. Rowan *et al.*, Physics Letters A 233, p. 303 (1997).

2. "The quality factor of natural fused quartz ribbons over a frequency range from 6 to 160 Hz," S. Rowan *et al.*, Physics Letters A 227, p.153 (1997).

3. “Investigations into the effects of electrostatic charge on the Q factor of prototype fused silica suspension for use in gravitational wave detectors,” S. Rowan *et al.*, Class. Quantum Grav. 14, p. 1537 (1997).

4. “Energy dissipation in the pendulum mode of the test mass suspension of a gravitational wave antenna,” V. B. Braginsky *et al.*, Physics Letters A 218, p. 164 (1996).

5. “Energy dissipation in violin modes of the test mass suspensions of gravitational-wave antennas,” Physics-Doklady 40 (11), p. 564, (1997).

6. “Brownian motion of a mass suspended by an anelastic wire,” G. I. Gonzalez and P. R. Saulson, J. Acoust. Soc. Am. 96 (1), p. 207 (July 1994).

7. Numerical Recipes in C, 2nd edition, W. H. Press *et al.*, Cambridge University Press, New York, 1992.

8. “The shape of fiber tapers,” T. A. Birks and Y. W. Li, Journal of Lightwave Technology 10 (4), p. 432 (April 1992).

APPENDIX 1 DERIVATION OF THE EQUATIONS OF MOTION

The equations of motion for the nonuniform anelastic wire pendulum are very similar to those for the uniform wire pendulum as presented by Gonzalez and Saulson [6]. The oscillation amplitudes are assumed small and shearing forces negligible. We consider motion only in the x-direction (the sensitive direction for the interferometer). The fiber has a displacement x(z,t) as a function of its length coordinate and time, and is rigidly clamped at its upper point to a rigid support and at its bottom point to the test mass. The wire is attached to the test mass a distance h from its center of gravity, so position of the test mass is $x_M(t)=x(L,t)+h\Phi(L,t)$, where $\Phi(t)=x'(L,t)$ is the rotation of the test mass. The test mass has mass M and moment of inertia J, and the fiber has linear mass density $\rho(z)$ and moment of inertia I(z).

We begin by constructing the Lagrangian for this system. The total kinetic energy is that of the motion of the wire and mass and that of the rotation of the mass

$$T = \int_0^L \frac{1}{2}\rho(z)[\dot{x}(z,t)]^2 dz + \frac{1}{2}M\dot{x}_M^2(t) + \frac{1}{2}J\dot{\Phi}^2(t)$$

The total potential energy is the sum of the gravitational potential energy, which is lossless

$$V_{grav} = \int_0^L \frac{1}{2}T[x'(z,t)]^2 dz + \frac{1}{2}Th\Phi^2(t)$$

and the elastic potential energy, which is lossy due to the structural damping, which enters as an imaginary component of the Young's modulus E

$$V_{el} = \int_0^L \frac{1}{2} EI(z)[x''(z,t)]^2 dz$$

We form the action

$$S = \int (T - V) dt$$

and set the variation of the action dS to zero with respect to x(z,t), $x_M(t)$, and $\Phi(t)$ to get the following terms:

$$\begin{aligned}
\delta \int dt \frac{1}{2} \int_0^L \rho [\dot{x}]^2 dz &= \int dt \int_0^L \rho \dot{x} \delta \dot{x} dz \\
&= \int_0^L \rho dz \int dt \dot{x} \delta \dot{x} \\
&= \int_0^L \rho dz [\dot{x} \delta x|_t^t - \int dt \ddot{x} \delta x] \\
&= -\int dt \int_0^L dz \rho \ddot{x} \delta x,
\end{aligned}$$

$$\delta\int dt\left(-\int_0^L \frac{1}{2}T[x']^2 dz\right) = -\int dt\int_0^L Tx'\delta x' dz$$

$$= \int dt\left[-(Tx'\delta x)\Big|_0^L + \int_0^L dz\, Tx''\delta x\right]$$

$$= \int dt\left[-Tx'(L)\delta x\Big|_L + \int_0^L dz\, Tx''\delta x\right],$$

$$\delta\int dt\left(-\frac{1}{2}E\int_0^L I[x'']^2\right) = -E\int dt\int_0^L dz\, Ix''\delta x''$$

$$= -E\int dt\left[(Ix''\delta x')\Big|_0^L - \int_0^L dz(I'x'' + Ix''')\delta x'\right]$$

$$= -E\int dt[I(L)x''(L)\delta x'\Big|_L - \{I'x'' + Ix'''\}\delta x\Big|_0^L]$$

$$-E\int dt\int_0^L dz(I''x'' + 2I'x''' + Ix^{iv})\delta x$$

$$= -E\int dt\{I(L)x''(L)\delta x'\Big|_L - I'(L)x''(L) + I(L)x'''(L)\delta x\Big|_L\}$$

$$-E\int dt\int_0^L dz(I''x'' + 2I'x''' + Ix^{iv})\delta x,$$

$$\delta\int dt\frac{1}{2}M\dot{x}_M^2 \;=\; \int dtM\dot{x}_M\delta\dot{x}_M \;=\; -\int dtM\ddot{x}_M\delta x_M,$$

$$\delta\int dt\frac{1}{2}J\dot{\Phi}^2 \;=\; -\int dtJ\ddot{\Phi}\delta\Phi,$$

$$\delta\int dt\frac{1}{2}Th\Phi^2 \;=\; \int dtTh\Phi\delta\Phi,$$

We can now use the fact that

$$\delta x\big|_L \;=\; \delta x_M - h\delta\Phi, \qquad\qquad \delta x'\big|_L \;=\; \delta\Phi,$$

and group similar terms to get

$$-E(I(z)x^{iv} + 2I'(z)x''' + I''(z)x'') + Tx'' \;=\; \rho\ddot{x},$$
$$E(I'(L)x''(L) + I(L)x'''(L)) - Tx'(L) \;=\; M\ddot{x}_M,$$
$$-E(hI(L)x'''(L) + hI'(L)x''(L) + I(L)x''(L)) \;=\; J\ddot{\Phi}$$

Finally, the boundary conditions at the top end of the fiber, where it is modelled as rigidly clamped, are:

$$x(0) \;=\; x'(0) \;=\; 0$$

APPENDIX 2 THE SHAPES OF FIBER TAPERS

It should be emphasized first that the fiber taper profiles used in this analysis have been based on theoretical derivations that use some simplifying assumptions, and that no actual tapered fibers

were analyzed. The results reported above should therefore be taken as indicative of the trends to be expected and the rough magnitude of the Q-reduction as taper length and end radius are varied. There is, of course, nothing to prevent actual fiber tapers from being measured and their profiles entered into the code.

Birks and Li [8] have presented a theory for the fabrication of nearly arbitrary taper shapes based on the model of a fiber that is uniformly heated within a certain region and pulled at a constant rate. The width of the hot zone is allowed to vary with the pull length. The authors dispense with the complicated hydrodynamics of viscous media by assuming that the heated region stretches uniformly and the unheated region does not stretch at all. This assumption is not tremendously restrictive, because it is well approximated by a small torch that oscillates repeatedly within the 'hot zone' region rapidly as the fiber is pulled. The width of the 'hot zone' can be varied by varying the torch oscillation amplitude. This technique is used in the manufacture of optically lossless optical fiber tapers.

If the taper extension (the length by which the fiber has been pulled) is x and the width of the hot zone as a function of taper extension is $W(x)=W_0+\alpha x$, where $-1<\alpha<1$, Birks and Li have shown that the radius of the fiber in the hot zone is

$$r(x) = r_o \exp\left[-\int_0^x \frac{1}{2}\frac{dx'}{W_0 + \alpha x'}\right]$$

The length of the taper z(x) is given by the formula

$$z(x) = \frac{1}{2}[x + W_0 - W(x)]$$

The case where $\alpha=0$ is that of the hot zone of constant width, and it is easy to show that in this case

$$r(z) = r_0 \exp\left(-\frac{z}{W_0}\right) = r_0 \exp\left(-\ln\left(\frac{r_0}{r_1}\right)\frac{z}{z_0}\right)$$

This is the exponential taper modelled in this analysis, and it is obtained by simply putting a rod into a torch flame and pulling. If $\alpha=-1/2$ (that is, the 'hot zone' shrinks at half the rate that the fiber is pulled), then it can be seen that the taper profile is

$$r(z) = r_0\left[1 - \frac{2z}{3W_0}\right] = r_0 - (r_0 - r_1)\left(\frac{z}{z_0}\right)$$

This is the linear taper modelled by the code. It is interesting to note that if the 'hot zone' grows at the same rate as the fiber is pulled (α=1), then the taper length is zero and the fiber has uniform radius up to the abrupt transition to the outer diameter. The case of a hand-drawn fiber, where a portion of the rod is heated in a flame, and then removed from the flame and rapidly pulled, will have the hot zone stretching with the fiber and cooling, and can be expected to be approximated by α somewhere between 0 and 1, depending on the relative importance of cooling radially at the fiber surface to cooling axially out the fiber ends.

The Glasgow group has manufactured many of their suspension fibers using a draw tower with a ring heater. Here, the rod stock is fed into the heater slowly, and the fiber drawn out of the heater quickly; the diameter reduction is simply related to the ratio of feed and draw speeds. Rather than model the detailed temperature profile within the heater and the hydrodynamics of the fibers as it necks down, we again make the simplifying assumption that the temperature is uniformly hot inside the heater and cold outside, and that the fiber stretches uniformly inside the heater. It is assumed that when the fiber is pulled to the final length that the feed and draw are abruptly stopped, so that the taper profile of the finished fiber is the same as that while the fiber is drawn.

Conservation of mass density flowing into and out of the heater yields the formula

$$r^2(z)v(z) = (r_0)^2 v_0 = (r_1)^2 v_1 = \text{constant}$$

If the fiber is uniformly stretched in the heater, then

$$\frac{dv}{dz} = \frac{(v_1 - v_0)}{z_0}$$

These two equations can be solved for the radius as a function of position in the hot zone:

$$r(z) = \frac{r_0}{\sqrt{1 + \left(\left(\frac{r_0}{r_1}\right)^2 - 1\right)\frac{z}{z_0}}}$$

The form of the inverse-square-root taper for constant taper length and varying taper depths is shown in Figure 8, justifying the analysis of the data in Figures 5 and 6.

Figure 8: The inverse-square-root taper profile. The taper depths are: solid line, .3 mm; dashed line, 1.2 mm; dotted line, 2.7 mm.